ACI STRUCTURAL JOURNAL TECHNICAL PAPER

Title no. 103-S07

Modeling of Unbonded Post-Tensioned Concrete Beams Critical in Shear

by Frank J. Vecchio, Paul Gauvreau, and Karen Liu

A stress-slip constitutive model is formulated for use with two-node bond-link elements to represent friction effects occurring in unbonded tendons of post-tensioned concrete beams. The friction effects considered are those arising from profile curvature and tendon wobble; thus, changes in tendon force during stressing, setting, and subsequent member loading are inherently modeled. The formulation is incorporated into a nonlinear finite element algorithm, where it is found to simulate friction effects well under all stages of stressing and loading. A series of shear-critical beams is modeled and analyzed; the load capacity, cracking patterns, and deformation response of all beams and the accompanying variations in tendon forces, are accurately simulated. It is shown that neglecting friction effects in unbonded post-tensioned beams has a minor influence on the computed response, whereas neglecting increases in tendon forces during loading has a major influence. Analyses based on code specifications tend to be overly conservative with respect to shear capacity and are marked by wide scatter.

Keywords: analysis; design; prestress; shear; tendon.

INTRODUCTION

Post-tensioned structural systems for short- and medium-span concrete bridges generally make inefficient use of the compressive strength of concrete. This occurs because the dimensions of the primary cross section are generally selected on the basis of code thickness requirements, detailing requirements, anchorage hardware, or rules-of-thumb, none of which directly consider the requirements of strength and serviceability in longitudinal flexure. The result is typically a structure in which the compressive stresses under service conditions are significantly less than allowable, and where the compression stress block at ultimate is significantly thinner than the flange or slab, even for relatively low-strength concrete. This practice is not only inefficient, it also provides little incentive to the use of high-strength concrete.

A challenge currently facing designers is to advance building and bridge technology through the development of new structural systems that take advantage of recent advances in materials technology. Various high-performance systems are being examined and developed worldwide. One option is through the use of external, unbonded prestressing; with the relatively large diameter post-tensioning ducts removed from within web elements, for example, thinner and more efficient sections can be developed. The behavior of such sections in shear, however, has not been extensively investigated and is not well understood.

Another concern lies in the rationality of some code provisions. For example, vertical web reinforcement in structures prestressed with unbonded tendons is currently dimensioned on the basis of code requirements developed for girders with bonded longitudinal reinforcement. The contribution of stirrups to the member's shear resistance is thus predicated on a load path in which the stirrups equilibrate the vertical component of a diagonal compressive force in the concrete (that is, internal truss action is established). For this transfer of force to take place, however, the horizontal component of the diagonal compression must be equilibrated by a change in the force in the longitudinal tensile reinforcement. By definition, however, the force in unbonded tendons is essentially constant between the anchors. Hence, the stirrups cannot contribute to shear resistance, according to the classical truss model, in girders containing no conventional longitudinal reinforcement. Arching of the effective prestress force has been identified as a valid mechanism for resisting shear in girders prestressed with unbonded tendons.[1] If one adopts this viewpoint, then stirrups cannot contribute directly to shear resistance via usual mechanisms, which is thus contrary to the design philosophy currently embodied in design codes.

Whether developing new high-performance designs, or invoking a rational approach to current design situations, a need exists for reliable and accurate tools in assessing the strength and behavior of shear-critical prestressed members with unbonded tendons. Application of nonlinear finite element procedures is one possible approach. Not only must the finite element program accurately model the shear behavior of cracked concrete, it must properly represent the nature of the forces developed in unbonded tendons, including the effects of friction during the stressing, anchoring, and loading stages.

RESEARCH SIGNIFICANCE

Current conceptual models for representing the shear resistance in members with unbonded tendons, as embodied in our design codes, are suspect. The reason is that unbonded longitudinal reinforcement cannot engage the stirrups in an internal-truss mechanism in the usual manner if the members contain no conventional longitudinal reinforcing bar. As new design approaches evolve, and as higher stress demands are placed on shear-resisting elements, tools are needed for accurately accessing the strength and behavior of shear-critical members prestressed with unbonded tendons. This paper presents a finite-element-based approach for modeling shear resistance in such members, with consideration given to friction effects.

FINITE ELEMENT FORMULATION

The force in a post-tensioning tendon generally diminishes inward from the jacking end due to friction losses arising

ACI Structural Journal, V. 103, No. 1, January-February 2006.
MS No. 04-273 received August 18, 2004, and reviewed under Institute publication policies. Pertinent discussion including author's closure, if any, will be published in the November-December 2006 *ACI Structural Journal* if the discussion is received by July 1, 2006.

Frank J. Vecchio, *FACI, is a professor of civil engineering at the University of Toronto, Toronto, Ontario, Canada. He is a member of Joint ACI-ASCE Committees 441, Reinforced Concrete Columns, and 447, Finite Element Analysis of Reinforced Concrete Structures. His research interests include nonlinear analysis and design of concrete structures, constitutive modeling, forensic analysis, and repair and rehabilitation of structures.*

Paul Gauvreau *is an associate professor of civil engineering at the University of Toronto. His research interests include the development of structural systems that make efficient use of modern materials, including high-strength concrete.*

ACI member **Karen Liu** *is a MASc candidate in the Department of Civil Engineering at the University of Toronto. Her interests include design of reinforced and prestressed concrete members including the use of the nonlinear analysis method.*

from tendon wobble and tendon curvature. The basis for the friction model adopted in the finite element formulation herein is the relationship described by Leonhardt.[2] Here, the tendon force variation along a span segment, between Points A and B in Fig. 1, is given by

$$T_B = T_A e^{-(\mu\alpha + KL_H)} \tag{1}$$

where T_A is the tendon force at Location A; T_B is the tendon force at Location B; L_H is the horizontal projection of the distance between A and B; α is the total angle change in the inclination of the tendon between Points A and B (in radians); K is the wobble coefficient; and μ is the curvature coefficient. Appropriate values for wobble coefficient and curvature coefficient are generally available from codes or from tendon suppliers. Note that in the typical post-tensioning operation, the tendon may be initially stressed beyond the desired final value and then relaxed. Also, there may be additional force lost due to setting of wedges during transfer of force from jack to anchor. Both actions will result in a reverse gradient of friction losses being established, with the tendon force generally peaking at some distance inward from the anchor point. The nature of the friction losses, however, can still be fully described by proper application of Eq. (1).

In a finite element context, the post-tensioning bars or tendons can be represented by truss bar elements. Bond-link elements can be used to connect the bar elements to solid elements representing the concrete beam (refer to Fig. 2). An appropriate bond stress-slip model can then be defined to describe the differential movement of the bar (tendon) elements relative to the surrounding concrete elements.

The bond-link element is a two-node nondimensional element, with the two nodes initially coincident; one node is connected to the solid elements representing the reinforced concrete beam and one node is connected to the truss elements representing the prestressing tendon. The link element can be oriented at any arbitrary angle θ to the horizontal, suitable in the case of inclined tendons. A general conceptual representation of a link element is shown in Fig. 3, consisting of two orthogonal springs.[4] One spring deforms tangentially to the truss elements, thus representing bond slip and bond stresses. The other spring deforms in a radial direction relative to the truss element, representing normal displacements. In representing post-tensioning tendons, the properties of the tangential spring are defined such that they describe frictional stresses rather than bond stresses. The normal spring, on the other hand, is assumed infinitely stiff (that is, no normal displacements permitted). The element stiffness matrix for the link element, with respect to tangential and normal displacements at each node (that is, $\{\Delta_{ti}, \Delta_{ni}, \Delta_{tj}, \Delta_{nj}\}$), is given as

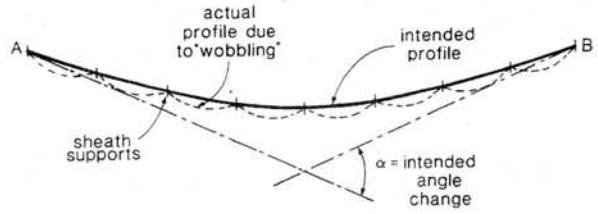

Fig. 1—Friction losses in unbonded tendon due to tendon wobble and curvature.[3]

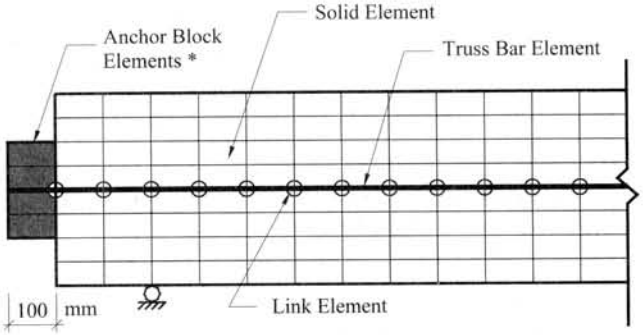

* α_c=0.010/° C in horizontal direction only

Fig. 2—Representation of unbonded tendons in fininte element context.

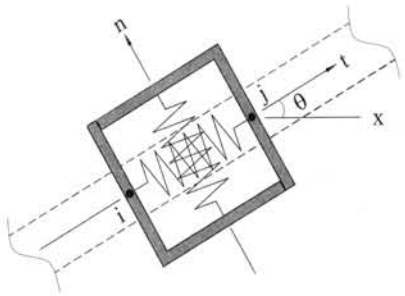

node i connected to truss elements (tendons)

node j connected to solid elements (concrete)

Fig. 3—Representation of bond-link element.[4]

$$[S]_m = \begin{bmatrix} K_t & 0 & -K_t & 0 \\ 0 & K_n & 0 & -K_n \\ -K_t & 0 & K_t & 0 \\ 0 & -K_n & 0 & K_n \end{bmatrix} \tag{2}$$

Standard transformations are used to redefine the stiffness matrix relative to the global coordinate system. Note that $K_n \to \infty$.

To account for friction losses due to wobble and curvature of the tendon, the bond stress model adopted is as shown in Fig. 4; that is, a constant stress τ_1 (either positive or negative) is assumed to act at any given slip displacement Δ. Hence, the frictional stresses thus described are independent of the magnitude of differential movement, but rather depend only on the direction of movement.

Based on a modification of Eq. (1), the magnitude of the frictional stress τ_1 for the link at Node *i* is by

$$\tau_1 = \frac{\Delta F}{LP_b} = \frac{f_{sp}A_{ps}}{P_b}\frac{[1 - e^{-(\mu\alpha + KL)}]}{L} \quad (3)$$

where f_{sp} is the tendon stress at Node i; A_{ps} is the cross-sectional area of the tendon; L is the length of tendon tributary to Node i; and P_b is the perimeter of the tendon cross section (which, for convenience, can be taken as 1.0). Note that the angle α in Eq. (3) is the angle subtended by the two in-framing truss bar elements at Node i (that is, zero if the truss bars are colinear; positive value if Node i is a harp point or if the tendon is draped). The angle θ, used to define the orientation of the link element, is set equal to an inclination half-way between the two in-framing truss elements.

A secant frictional stiffness factor, corresponding to a total slip of Δ_1, is effectively defined as

$$k_1 = \tau_1/\Delta_1 \quad (4)$$

The tangential stiffness coefficient in the element stiffness matrix is thus defined as

$$K_t = k_1 \cdot L \cdot P_b \quad (5)$$

This formulation is suitable for direct implementation into a nonlinear algorithm based on a secant stiffness approach (as used in this study). Alternative formulations can readily be developed for tangent stiffness-based algorithms. It should also be noted that once the incremental slip reverses direction (for example, as a result of draw-back during set), the frictional shear stress reversed direction as well. Consequently, the friction may be acting in the direction opposite to the that of the net slip (for example, point corresponding to Δ_2 in Fig. 4). In this case, the coefficients k_1 and K_t will have negative values.

To facilitate finite element modeling of the jacking and setting operations, and the resulting tendon forces and associated friction losses, a consistent loading scheme is required. The approach used here is to define an anchorage block within the finite element mesh (refer to Fig. 2) to which the tendon end is attached. The elements forming the anchorage block are given a convenient coefficient of thermal expansion for unidirectional expansion in the axial direction of the member. Temperature strains can then be imposed on the anchorage elements to simulate draw-out of the tendon during jacking, and draw-back during setting. For example, if the anchorage block is made 100 mm thick and given a coefficient of thermal expansion in the x-direction of 0.010/°C, then imposing a differential temperature that increases from 0 to 30 °C and then drops back to 24 °C will produce a tendon draw-out of 30 mm followed by a 6 mm draw-back due to setting. Tendon stresses and friction losses will then be automatically computed within the finite element analysis according to the stress formulations presented.

The formulations described above were implemented into a nonlinear finite element program for analysis of two-dimensional reinforced-concrete solid structures. The material behavior models implemented in the program are based on the Disturbed Stress Field Model,[5] which is an extension of the Modified Compression Field Theory.[6] In it, cracked reinforced concrete is treated as an orthotropic material based on the concept of smeared rotating cracks.

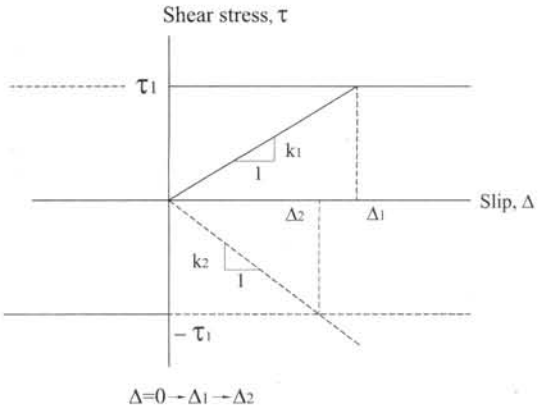

Fig. 4—Bond stress model used to represent frictional shear stresses acting on unbonded tendons.

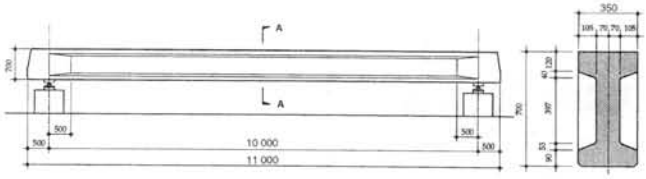

(a) elevation and cross section

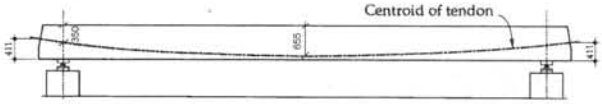

(b) tendon profile

Fig. 5—Details of Gauvreau test girders.[1]

ANALYSIS OF FLEXURE-DOMINATED BEAM SPECIMENS

In addition to the frictional stresses incurred in unbonded tendons during the post-tensioning and setting phases, local frictional effects can also develop during later loading phases. In particular, as a member is loaded and develops flexural cracks, and consequently as the tendon elongates, stresses in the tendon will increase on average but will be slightly greater in the vicinity of large flexural cracks. Friction prevents the increase in tendon strain from being uniformly distributed along its length. Hence, with respect to variation in tendon stresses along an unbonded tendon, the effects of friction will be more pronounced in flexure-dominant members. For this reason, a series of specimens heavily influenced by flexural action would be examined first in testing the proposed model's ability to represent tendon friction effects accurately.

The series of four girders tested by Gauvreau[1] was selected for this study: Beams S1, S2, S3, and S4. Each of the I-girders had an overall depth of 700 mm and spanned 10 m, with a flange thickness of 350 mm and a web thickness of 140 mm (refer to Fig. 5). Each girder in this series was post-tensioned using a single unbonded tendon with a parabolic profile. The BBRV stressing system consisted of 7-mm diameter wires, housed in a smooth 40-mm diameter smooth duct, and was stressed from one end only. In addition, each girder contained various amounts of conventional longitudinal reinforcement and shear reinforcement. Specimen details and material properties are given by Gauvreau.[1]

Each girder was tested by static loading at midspan in a displacement-controlled mode. In all four girders, large

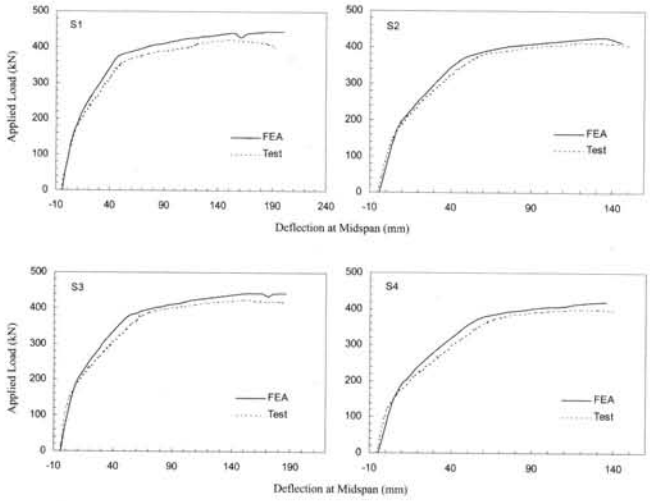

Fig. 6—Comparison of calculated and measured load-deflection responses for Gauvreau test girders.

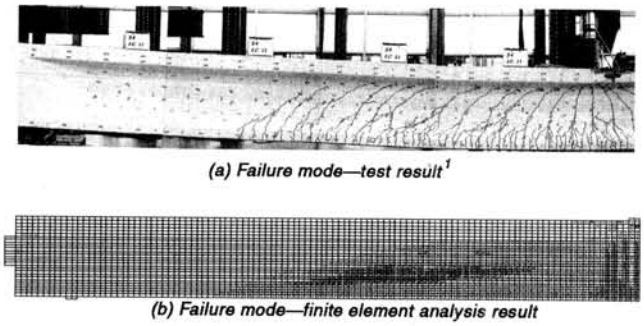

(a) Failure mode—test result[1]

(b) Failure mode—finite element analysis result

Fig. 7—Crack patterns and failure mode for Gauvreau Specimen S4.

flexural cracks developed in the central portion of the girders to approximately 3 m on either side of the midspan, with crack widths of up to 3.5 mm in width. Crushing and spalling of concrete was observed in the compression zone at the ultimate load stage. Beams S1, S2, and S3 experienced a compression-flexure failure mode; Specimen S4 failed by sudden rupture of stirrups at various locations within 1.0 m of the midspan.

A finite element (FE) model was developed to represent the test specimens; due to symmetry, only 1/2 of each beam was modeled. A typical mesh of 110 x 27 eight-degree-of-freedom rectangular elements was used to represent the girders; all the longitudinal reinforcement and prestressed reinforcement was represented by truss elements, while the shear reinforcement was modeled as smeared. The truss elements representing the prestressing steel were connected to the concrete elements by link elements. To model the frictional effects, a curvature coefficient of 0.05 and a wobble coefficient of between 0.000610/m and 0.000653/m were used. The FE analysis was conducted in two stages. First, the tendon was progressively stretched until the tendon stress matched that in each test girder, as measured by load cells installed at the anchor points. At that point, the tendon draw-out was fixed constant. Then, a monotonically-increasing downward displacement was imposed at the midspan of the girder, with a typical step size of 5 mm.

The finite element analyses were able to provide highly accurate calculations of the response of these test specimens. Shown in Fig. 6 are comparisons between the calculated and observed load-deflection response of the girders. The pre- and

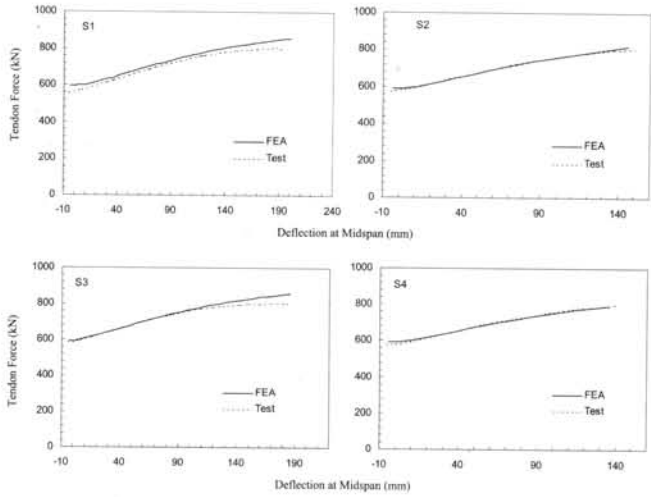

Fig. 8—Comparison of calculated and measured tendon forces for Gauvreau test girders.

post-cracking stiffness, ultimate load capacities, and displacements at peak load are captured. The crack patterns, crack widths, and failure modes were also well predicted (refer to Fig. 7). Perhaps most significant, however, is the close correlation obtained for the tendon force as it increased with deflection of the girders (refer to Fig. 8). Because this tendon force was influenced by frictional effects, both in the test and in the analyses, this close correlation provides confidence in the friction modeling implemented into the FE formulation. Table 1 summarizes the strong correlations obtained in the calculations of ultimate load, force in the tendon at ultimate load, and midspan deflection at ultimate load.

ANALYSIS OF SHEAR-DOMINANT BEAM SPECIMENS

To corroborate the proposed formulation's ability to model post-tensioned unbonded structures critical in shear, two sets of beam specimens tested by Kordina et al.[7] and Kordina and Hegger[8] were examined. The first set, comprising Beams B1, B2, and B3, were simply supported beams with a span of 4.0 m. Beams B1 and B2 had an I-shaped cross section, whereas Beam B3 was T-shaped. Beams B1 and B2 contained three straight unbonded post-tensioning bars (26 mm diameter Dywidag) within the bottom flange, whereas Beam B3 had three layers of harped tendons (six 0.6 in. VSL monostrand) within the web. All three specimens additionally contained various amounts of conventional longitudinal reinforcement and shear reinforcement. Details of the specimens are given in Fig. 9(a). The beams were subjected to monotonically increasing load applied at the midspan.

The second set of specimens tested by Kordina and Hegger[8] included Beams B4, B5, B6, B7, and B8. All beams in this series were I-shaped in cross section, 740 mm in total depth, and simply supported spanning 6.0 m. Beams B4, B5, and B6 each contained one straight prestressing bar in the top flange (26-mm diameter Dywidag) and three straight prestressing bars in the bottom flange (three 26 mm-diameter Dywidag for B4 and B5, three 32-mm diameter Dywidag for B6). Beams B7 and B8 contained one straight prestressing bar in the top flange (26-mm diameter Dywidag) and 10 harped tendons in the bottom flange and web (ten 0.6 in. VSL monostrand). Again, all specimens contained various amounts of conventional longitudinal reinforcement and

Table 1—Results of Gauvreau[1] test girders—friction considered

Girder	$T_{pi,test}$, kN	$T_{pi,FEA}$, kN	$T_{pi,FEA}/T_{pi,test}$	$T_{pu,test}$, kN	$T_{pu,FEA}$, kN	$T_{pu,FEA}/T_{pu,test}$	$P_{u,test}$, kN	$P_{u,FEA}$, kN	$P_{u,FEA}/V_{u,test}$	$\Delta_{u,test}$, mm	$\Delta_{u,FEA}$, mm	$\Delta_{u,FEA}/\Delta_{u,test}$
S1	592	597	1.01	791	817	1.03	422	441	1.04	149.7	150.9	1.01
S2	592	591	1.00	787	805	1.02	413	428	1.04	123.0	135.9	1.10
S3	592	589	0.99	799	838	1.05	423	443	1.05	150.5	160.9	1.07
S4	592	593	1.00	782	784	1.00	398	416	1.05	120.1	125.6	1.05
		Mean	1.00		Mean	1.03		Mean	1.04		Mean	1.06
		Standard deviation	0.01		Standard deviation	0.02		Standard deviation	0.01		Standard deviation	0.04
		COV, %	0.61		COV, %	1.91		COV, %	0.50		COV, %	3.85

Note: COV = coefficient of variation.

shear reinforcement. Additional specimen details are given in Fig. 9(b). These beams differed from the first set in that three separate loading cases were applied to each. The first loading condition saw two concentrated loads applied at the third-points of the simply supported full-span beam. The second loading stage had a concentrated load applied at one of the third-points of the full-span beam, whereas the third condition involved a concentrated load applied at the midspan of partially cantilevered beams. The shear reinforcement details and loading conditions were such that each loading conditions produced an independent failure zone. In total, 15 tests were conducted.

It was reported by Kordina et al.[9] that all beams in this series were governed by shear-critical behavior. Beam B2 failed by sudden web crushing, and Beam B3 experienced web crushing failure in the tension chord region near a support. All others failed in tension shear or flexural shear.

In developing finite element models for this series of beam, the entire lengths of the beams had to be modeled owing to the unsymmetrical reinforcement and loading details. All longitudinal reinforcement and prestressing reinforcement were modeled with truss bar elements, and all shear reinforcement was modeled as smeared. Again, unbonded tendons were simulated using linkage elements to connect between the tendons and the concrete elements at various locations along the span. A curvature coefficient of 0.15 and a wobble coefficient of 0.0005/m were used in modeling the friction effects in the Dywidag bars. A curvature coefficient of 0.20 and a wobble coefficient of 0.0035/m were used in modeling friction effects in the harped tendons.

The finite element meshes developed typically contained a grid of 88 x 18 rectangular elements for the 4.0 m beams, and 130 x 17 rectangular elements for the 6.0 m beams. The analyses were conducted in two stages. First, the stress in the tendons was progressively increased until it matched the initial tendon stress in each test girder, and then the tendon was allowed to draw-back 6 mm before fixing. Then, a monotonically increasing downward displacement was imposed in a manner corresponding to the test condition, with a typical step size of 0.25 mm (for 4.0 m beams) or 0.5 mm (for 6.0 m beams). It should be noted that in the second and third test conditions of Beams B4 through B8, the analyses began with the specimens assumed undamaged whereas in the actual tests, the beams had experienced some cracking due to previous loading.

The ultimate load capacities and tendon forces calculated from the finite element analyses are compared to the experimental results in Table 2 for all 15 tests performed. The ratio of calculated-to-measured strengths of the beams had a mean value of 1.01 and a coefficient of variation of 6.5%, indicating

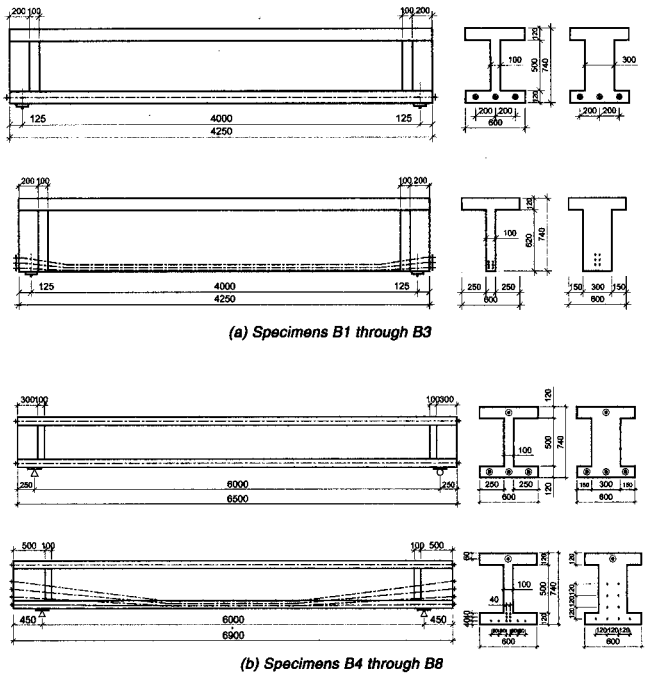

Fig. 9—Details of beams tested by Kordina et al.[7,8]

that the shear-critical mechanisms governing these specimens were well simulated. The calculated tendon forces at ultimate were also were reasonably accurate. For all 15 tests, the correct modes of failure were calculated, ranging from web-shear to flexural-shear. The predicted crack patterns were also in good agreement with test observations (refer to Fig. 10) bearing in mind that some segments of the test beams were precracked due to previous loading under different conditions.

INFLUENCE OF FRICTION

The analyses described above considered friction effects on the initial tendon force profiles within the beams and on the local changes in tendons forces arising from member loading. If frictional effects were ignored, the tendon forces would be uniform along the lengths of the beams at all times. To assess the extent to which friction influences shear response, both series of beams were reanalyzed assuming no frictional stresses developed (for example with τ_1 in Eq. (3) set to zero for all levels of slip).

In the flexure-dominated girders tested by Gauvreau,[1] ignoring friction effects resulted in a slight deterioration in the accuracy of the computed response. The ultimate load capacity and the force in the tendon at ultimate limit state were slightly higher estimated relative to the results of the

Table 2—Results of Kordina et al. test beams—friction considered

Beam	$T_{pi,test}$, kN	$T_{pi,FEA}$, kN	$T_{pi,FEA}/T_{pi,test}$	$T_{pu,test}$, kN	$T_{pu,FEA}$, kN	$T_{pu,FEA}/T_{pu,test}$	$V_{u,test}$, kN	$V_{u,FEA}$, kN	$V_{u,FEA}/V_{u,test}$	$\Delta_{u,FEA}$, mm	Failure mode—test	Failure mode—FEA
B1	380	389	1.02	596	484	0.81	225	220	0.98	4.05	T-S/F-S	T-S/F-S
B2	700	717	1.02	1112	1120	1.01	400	424	1.06	10.9	W-C	W-C
B3	784	728	0.93	994	1026	1.03	338	310	0.92	10.1	W-C	W-C
B4-1	948	921	0.97	1319	1316	1.00	375	366	0.98	14.2	T-S/F-S	T-S/F-S
B4-2	1159	1167	1.01	1435	1598	1.11	483	471	0.97	22.0	T-S/F-S	T-S/F-S
B4-3	1070	1073	1.00	1347	1358	1.01	425	420	0.99	12.0	T-S/F-S	T-S/F-S
B5-1	1389	1405	1.01	1743	1913	1.10	550	573	1.04	18.2	T-S/F-S	T-S/F-S
B5-2	1330	1325	1.00	1771	2045	1.15	650	668	1.03	24.7	T-S/F-S	T-S/F-S
B6-1	1349	1346	1.00	1730	2197	1.27	550	651	1.18	27.9	T-S/F-S	T-S/F-S
B6-2	1460	1463	1.00	1788	2179	1.22	650	660	1.02	25.5	T-S/F-S	T-S/F-S
B6-3	1276	1266	0.99	1400	1503	1.07	475	464	0.98	8.4	T-S/F-S	T-S/F-S
B7-1	1030	1029	1.00	1352	1588	1.17	437	442	1.01	29.0	T-S/F-S	T-S/F-S
B7-3	941	930	0.99	1003	1079	1.08	325	315	0.97	8.3	T-S/F-S	T-S/F-S
B8-1	1395	1400	1.00	1790	2223	1.24	575	640	1.11	49.5	T-S/F-S	T-S/F-S
B8-3	1310	1299	0.99	1372	1512	1.10	437	433	0.99	11.0	T-S/F-S	T-S/F-S
		Mean	1.00		Mean	1.09		Mean	1.01			
		Standard deviation	0.02		Standard deviation	0.12		Standard deviation	0.07			
		COV, %	2.29		COV, %	10.59		COV, %	6.47			

Note: T-S/F-S = tension shear/flexural shear, and W-C = web crushing.

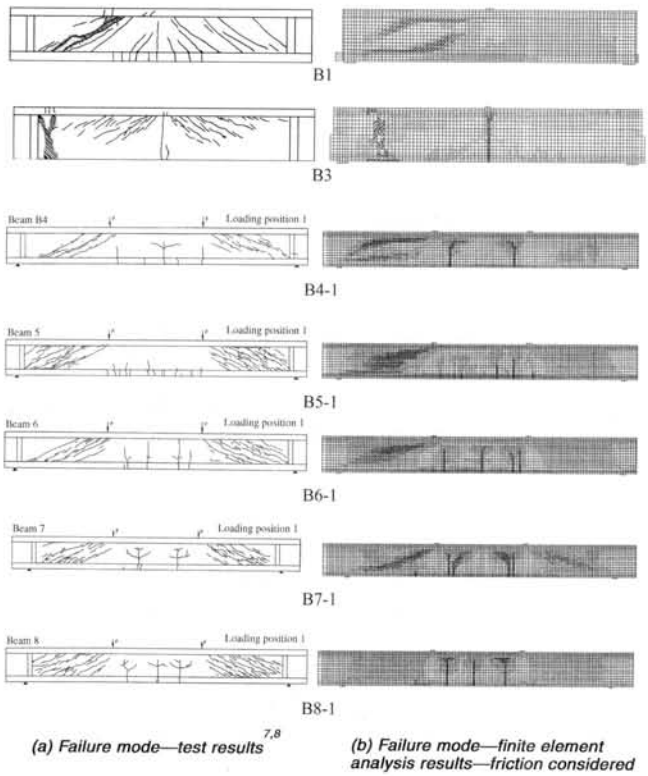

Fig. 10—Comparison of crack patterns and failure modes for typical Kordina et al.[7,8] test beams.

previous analysis (by only about 2% on average). The ductility of the beams, as measured by the midspan deflection at ultimate load, was considerably over-estimated; much more so than when friction is considered.

A similar pattern was observed when the shear-critical beams tested by Kordina et al.[7,8] were reanalyzed with friction effects ignored. The load capacity and tendon forces were slightly more over-estimated, relative to the experimental values, than when friction effects were considered. The degree of influence is minor, however, at approximately 2 to 3% relative to the more rigorous analyses. Hence, if the means to include frictional effects in the finite element analyses is not available, the deterioration in accuracy is not severe.

INFLUENCE OF INCREASING TENDON FORCES

In the analysis of post-tensioned members with unbonded tendons, it is common to represent the post-tensioning with externally applied end forces at the anchor locations and deviation forces at harp points or along a curvilinear segment. The presence of the tendon is then omitted in any subsequent sectional analysis. The post-tensioning forces are usually held constant, and hence do not account for the increase in tendon forces that will arise as the tendon in a loaded member undergoes further straining.

The Kordina et al.[7,8] beams were reanalyzed with the elements representing post-tensioning bars and tendons removed, and with external anchor and deviation point forces of constant magnitude applied. The applied forces were proportioned according to the initial post-tensioning forces. The analysis results showed that the calculated ultimate load capacity of the beams is significantly reduced by about 24% on average. Whereas previously the mean of the ratio of the calculated-to-measured strength for these beams was 1.01, it was reduced to 0.77 and accompanied by a doubling of the coefficient of variation (that is, much more scatter). Moreover, whereas the previous analyses correctly predicted a shear failure for all beams, several of the beams are now found to sustain a flexure-controlled failure mode. The indication is that increasing tendon forces cause a more rapid elevation in flexural capacity than they do in shear capacity. Hence, ignoring increasing tendon forces may result in a false, and potentially dangerous, conclusion that a member is flexure-critical and not likely to sustain a shear failure.

Table 3—Code-calculated strength for Kordina et al. beams

Specimen	V_{test}, kN	V_{FEA}, kN	V_{test}/V_{FEA}	V_{CSA}, kN	V_{test}/V_{CSA}	V_{AASHTO}, kN	V_{test}/V_{AASHTO}	$V_{ACI318\text{-}02}$, kN	V_{test}/V_{ACI}*	V_{test}/V_{ACI}†	V_{test}/V_{CEB}‡
B1	225	220	1.02	164	1.38	156	1.44	184	1.22	1.27	1.40
B2	400	424	0.94	398	1.01	—§	—§	354	1.13	1.23	0.89
B3	338	310	1.09	302	1.12	—§	—§	364	0.93	0.83	0.71
B4-1	375	366	1.02	213	1.76	213	1.76	277	1.35	1.26	1.29
B4-2	483	471	1.03	311	1.56	320	1.51	396	1.22	1.28	1.19
B4-3	425	420	1.01	360	1.18	335	1.27	349	1.22	1.14	1.24
B5-1	550	573	0.96	369	1.49	375	1.47	440	1.25	1.20	1.41
B5-2	650	668	0.97	489	1.33	493	1.32	581	1.12	1.07	1.29
B6-1	550	651	0.84	434	1.27	432	1.27	515	1.07	1.08	1.26
B6-2	650	660	0.98	560	1.16	—§	—§	538	1.21	1.20	1.19
B6-3	475	464	1.02	382	1.24	360	1.32	373	1.27	1.21	1.47
B7-1	437	442	0.99	278	1.57	261	1.67	332	1.32	1.09	1.28
B7-3	325	315	1.03	230	1.41	192	1.69	262	1.24	1.19	1.39
B8-1	575	640	0.90	383	1.50	375	1.53	459	1.25	1.22	1.17
B8-3	437	433	1.01	316	1.38	294	1.49	342	1.28	1.12	1.39
		Mean	0.99		1.36		1.48		1.21	1.16	1.24
		Standard deviation	0.06		0.20		0.17		0.11	0.11	0.20
		COV, %	6.08		14.77		11.25		8.83	9.83	16.34

*Measured-to-calculated strength using ACI 318-02.[13]
†Measured-to-calculated strength using ACI 318-83.[7]
‡Measured-to-calculated strength using CEB code.[7]
§High shear ratio ($A_v f_y / b_w s$); exceeds AASHTO code limit of 0.25.[11,12]

STRENGTHS ACCORDING TO CODE PROCEDURES

The shear strength calculation procedures for unbonded prestressed beams from three North American codes were examined: the Canadian code,[10] the AASHTO Code,[11,12] and the ACI Code (ACI 318-2002).[11] Each is cast in a form in which shear strength is derived from a steel contribution and a concrete contribution, although the manner in which these are calculated, and the limits imposed, vary somewhat. In all cases, material resistance factors or capacity reduction factors were set to 1.0 to produce a best-estimate of the strength of the test beams.

The ultimate shear capacities of the shear-critical beams tested by Kordina et al.[7,8] were calculated according to the code procedures. The shear strengths of each beam, as calculated by all three methods, are listed in Table 3, wherein they are compared to the experimental results and the results obtained from the finite element analyses. In the calculations using the AASHTO procedure, Beams B2, B3, and B6-2 exceeded the limit on the shear reinforcement ratio and hence their strengths could not be calculated.

In general, the code calculated values significantly underestimated the shear strengths. The ratio of measured-to-calculated strength has a mean value of 1.36 for the CSA method, 1.48 for the AASHTO method, and 1.21 for the ACI method. Moreover, the coefficients of variations for the mean strength were high for the three methods; 15, 11, and 9%, respectively. Hence, all three code procedures were somewhat unreliable, although conservative. In contrast, the strengths computed by finite element analyses had a mean ratio of 0.99 and a coefficient of variation of 6%, and thus considerably more accurate.

CONCLUSIONS

Based on the results of this limited study, the following conclusions are derived:

1. Friction losses in unbonded prestressing tendons can be effectively modeled in a finite element analysis context through use of bond-link elements and an appropriately modified bond-slip model;
2. Frictional effects that can be modelled include those arising from initial jacking, from anchor set, and from subsequent member loading;
3. Nonlinear finite element analyses that properly consider variations in tendon force can be used to accurately assess the strength, load-deformation response, ductility, cracking pattern, and failure mode of shear-critical unbonded post-tensioned members. To do so, however, the analyses must also include a reliable constitutive model for reinforced concrete behaviour in shear; for example, the Modified Compression Field Theory;
4. Ignoring friction effects (that is, assuming a uniform tendon force throughout the length of the member) results in only a minor deterioration in the accuracy of the analyses;
5. Ignoring tendon force increases due to additional straining under member loading (that is, treating the post-tensioning as constant, externally-applied forces) results in a significant under-estimation of load capacity in shear-critical beams. In some cases, the failure mode is also incorrectly determined; and
6. North American codes typically provide overly-conservative estimates of the strengths of shear-critical unbonded prestressed members, and with a wide scatter in comparison to observed strengths.

ACKNOWLEDGMENTS

This work was partially funded through a grant from the Cement Association of Canada. Their support is gratefully acknowledged.

NOTATION

f_{sp} = tendon stress at Node i
K = wobble coefficient per foot or per meter of tendon
K_n = stiffness of normal spring
K_t = stiffness of tangential spring
k_1 = secant frictional stiffness factor
L = length of tendon tributary to Node i
L_H = horizontal projection of the distance between A and B
P_b = the perimeter of the tendon cross section
P_u = applied load at ultimate loading stage
S_m = element stiffness matrix for the link element
T_A = tendon force at Location A
T_B = tendon force at Location B
T_{pi} = initial prestressing force in tendon
T_{pu} = prestressing force in tendon at ultimate loading stage
V_u = shear force at ultimate loading stage
α = total angle change in inclination of tendon between Points A and B, in radians
α_1 = slip corresponding to bond stress τ_1
Δ_2 = slip corresponding to bond stress τ_2
Δ_{ni} = normal displacement at Node i
Δ_{nj} = normal displacement at Node j
Δ_{ti} = tangential displacement at Node i
Δ_{tj} = tangential displacement at Node j
Δ_u = deflection of midspan at ultimate loading stage
μ = friction coefficient
θ = orientation of link element
τ_1 = bond stress

REFERENCES

1. Gauvreau, D. P., "Load Tests of Concrete Girders Prestressed with Unbonded Tendons," *Report* No. 194, Institute of Structural Engineering ETH Zurich, Birkh ser Publishers, 1992, 239 pp.

2. Leonhardt, F., "Prestressed Concrete Design and Construction, Wilhelm Ernst & Sohn, Berlin, 1964, 677 pp.

3. Collins, M. P., and Mitchell, D., *Prestressed Concrete Structures*, Response Publications, Canada, 1997, 766 pp.

4. Ngo, D., and Scordelis, A. C., "Finite Element Analysis of Reinforced Concrete Beams," ACI JOURNAL, *Proceedings* V. 64, No. 3, Mar. 1967, pp. 152-163.

5. Vecchio, F. J., "Disturbed Stress Field Model for Reinforced Concrete: Formulation," *Journal of Structural Engineering*, ASCE, V. 126, No. 9, Sept. 2000, pp. 1070-1077.

6. Vecchio, F. J., and Collins, M. P., "The Modified Compression-Field Theory for Reinforced Concrete Elements Subjected to Shear," ACI JOURNAL, *Proceedings* V. 83, No. 2, Mar.-Apr. 1986, pp. 219-231.

7. Kordina, K.; Hegger, J.; and Teutsch, M., "Application of Prestressed Concrete with Unbonded Tendons (Anwendung der Vorspannung ohne Verbund)," Bulletin No. 355, *Deutscher Ausschuss f Stahlbeton*, Berlin, 1984, pp. 71-133. (in German)

8. Kordina, K., and Hegger, J., "Shear-Carrying Behaviour of Prestressed Concrete Girders with Unbonded Tendons (Schubtragverhalten von Spannbetonbauteilen mit Vorspannung ohne Verbund)," Bulletin No. 381, *Deutscher Ausschuss f Stahlbeton*, Berlin, 1987, pp. 5-72. (in German)

9. Kordina, K.; Hegger, J.; and Teutsch, M., "Shear Strength of Prestressed Concrete Beams with Unbonded Tendons," *Journal of Structural Engineering*, ASCE, V. 86, No. 2, 1989, pp. 143-149.

10. Canadian Standards Association, "Design of Concrete Structures," *CSA Standard A23.3-200*, Clause 11 Shear and Torsion, May 2004, 18 pp.

11. American Association of State Highway Transportation Officials, "ASHTO LRFD Bridge Design Specifications and Commentary," 2nd Edition, Washington D.C., 1998, pp. 5-26.

12. American Association of State Highway Transportation Officials, "ASHTO LRFD Bridge Design Specifications and Commentary," 2000 Interim Edition, Section 5—Concrete Structures (SI), 2000, pp. 5-72.

13. ACI Committee 318, "Building Code Requirements for Structural Concrete (ACI 318-02) and Commentary (318R-02)," American Concrete Institute, Farmington Hills, Mich., 2002, pp. 139-186.